Human Molecular Genetics, 2017, Vol. 26, No. 23 4617–4628

doi: 10.1093/hmg/ddx344
Advance Access Publication Date: 4 September 2017
Original Article

ORIGINAL ARTICLE

The mitochondrial metallochaperone SCO1 maintains CTR1 at the plasma membrane to preserve copper homeostasis in the murine heart

Zakery N. Baker[1], Kimberly Jett[1], Aren Boulet[1], Amzad Hossain[1], Paul A. Cobine[2], Byung-Eun Kim[3], Amr M. El Zawily[1], Ling Lee[4], Glen F. Tibbits[4], Michael J. Petris[5] and Scot C. Leary[1,*]

[1]Department of Biochemistry, University of Saskatchewan, Saskatoon, Saskatchewan S7N 5E5, Canada, [2]Department of Biological Sciences, Auburn University, Auburn, AL 36849, USA, [3]Department of Animal and Avian Sciences, University of Maryland, College Park, MD 20742, USA, [4]Department of Cardiovascular Sciences, BC Children's Hospital Research Institute, Vancouver, BC V5Z 4H4, Canada and [5]Department of Biochemistry, University of Missouri, Columbia, MO 65211, USA

*To whom correspondence should be addressed at: Department of Biochemistry, University of Saskatchewan, Health Sciences Building, Rm 4D10, 107 Wiggins Road, Saskatoon, SK S7N 5E5, Canada. Tel: 3069664349; Fax: 3069664298; Email: scot.leary@usask.ca

Abstract

SCO1 is a ubiquitously expressed, mitochondrial protein with essential roles in cytochrome *c* oxidase (COX) assembly and the regulation of copper homeostasis. *SCO1* patients present with severe forms of early onset disease, and ultimately succumb from liver, heart or brain failure. However, the inherent susceptibility of these tissues to *SCO1* mutations and the clinical heterogeneity observed across *SCO1* pedigrees remain poorly understood phenomena. To further address this issue, we generated *Sco1*$^{hrt/hrt}$ and *Sco1*$^{stm/stm}$ mice in which *Sco1* was specifically deleted in heart and striated muscle, respectively. Lethality was observed in both models due to a combined COX and copper deficiency that resulted in a dilated cardiomyopathy. Left ventricular dilation and loss of heart function was preceded by a temporal decrease in COX activity and copper levels in the longer-lived *Sco1*$^{stm/stm}$ mice. Interestingly, the reduction in copper content of *Sco1*$^{stm/stm}$ cardiomyocytes was due to the mislocalisation of CTR1, the high affinity transporter that imports copper into the cell. CTR1 was similarly mislocalized to the cytosol in the heart of knockin mice carrying a homozygous G115S substitution in *Sco1*, which in humans causes a hypertrophic cardiomyopathy. Our current findings in the heart are in marked contrast to our prior observations in the liver, where *Sco1* deletion results in a near complete absence of CTR1 protein. These data collectively argue that mutations perturbing SCO1 function have tissue-specific consequences for the machinery that ultimately governs copper homeostasis, and further establish the importance of aberrant mitochondrial signaling to the etiology of copper handling disorders.

Received: June 26, 2017. **Revised:** August 21, 2017. **Accepted:** August 31, 2017

Introduction

Copper is an essential micronutrient that can rapidly cycle between two redox states, Cu^{+} and Cu^{2+}, thereby facilitating electron transfer. This property has been co-opted by a number of proteins which use copper as a cofactor to catalyze biochemical reactions critical to respiration, free radical detoxification, iron homeostasis, and neurotransmitter and collagen biosynthesis (1,2). Copper is also extremely toxic in excess because it can destabilize iron-sulphur clusters (3,4) and potentiate the generation of highly damaging free radicals (5,6). Conserved mechanisms therefore evolved to mitigate its toxic potential, and act in concert to regulate total and bioavailable copper stores such that the cell contains negligible amounts of the free metal ion (7). Genetic lesions or environmental insults that impair these copper handling mechanisms perturb copper homeostasis, and underlie a number of severe forms of human disease (8).

In mammals, copper enters the cell through the essential protein CTR1, the only known high-affinity copper importer (9,10). CTR1 functions as a homotrimer to facilitate copper translocation across the plasma membrane (11). Copper is then transferred to evolutionarily conserved, soluble chaperones that deliver it to various subcellular compartments (12–16). CTR1 abundance and localisation are tightly controlled to regulate the rate of copper import and, by extension, cellular copper homeostasis. Under conditions of copper excess, CTR1 can be internalized from the plasma membrane into endosomes (17), a mechanism that is thought to protect the cell from copper toxicity (18). Endosomally-localized CTR1 can then be targeted for degradation by the proteasome, or recycled back to the plasma membrane (19). However, the universality of this regulatory mechanism has been debated, given that CTR1 localisation is not always altered in response to increased copper concentrations (20). The P-type ATPases ATP7A and ATP7B normally reside in the trans-Golgi network where they promote the metallation of secreted cuproproteins (21–23). However, both proteins also undergo regulated trafficking to the cell periphery where they facilitate copper export (24,25). Pathogenic mutations in ATP7A and ATP7B severely perturb protein function and cause Menkes and Wilson disease, respectively (26,27).

There is a growing appreciation for the influence of mitochondria on how the cell senses its copper status and prioritizes its copper stores to maintain homeostasis (28). Mitochondria contain two enzymes that depend on copper for their activity; cytochrome *c* oxidase (COX) and a small, but physiologically significant fraction of copper-zinc superoxide dismutase (SOD1). COX contains two copper prosthetic groups (Cu_A, Cu_B) that are matured within the intermembrane space of the mitochondrion in biochemical reactions that require a surprisingly large number of accessory proteins termed COX assembly factors. Pathogenic mutations in genes encoding three of these factors, *COA6*, *SCO1* and *SCO2*, impair copper delivery to the Cu_A site of COX and result in a severe, isolated COX deficiency that underlies a number of early onset forms of fatal human disease (29–31). SCO1 and SCO2 are paralogs with complementary but non-overlapping functions in this pathway that rely on the ability of each protein to bind copper (32,33). *SCO* gene mutations also impair the function of a redox-dependent, mitochondrial signaling pathway that is integral to the regulation of cellular copper homeostasis, and affected tissues in *SCO1* and *SCO2* patients are both COX and copper deficient (34–36).

Three pedigrees with pathogenic mutations in *SCO1* have been described to date, each with a unique clinical phenotype and course of disease that selectively affects liver (30; P174L/R149X), heart (36; G132S/G132S) and/or brain (37; M294V/Y93X) function. How different mutations in a ubiquitously expressed gene produce such striking clinical heterogeneity remains an enduring mystery. Affected *SCO1* patient tissues are severely copper deficient, and the copper deficiency in *SCO1* and *SCO2* patient fibroblasts is driven in large part by a disproportionate rate of copper efflux from the cell (34). In contrast, loss of SCO1 function in the liver of a mouse model of the human disease results in a severe copper deficiency that is caused by a significant reduction in CTR1 abundance, and therefore copper uptake (38). These observations suggest that differences may exist across cell types in how SCO1-dependent mitochondrial signaling is integrated into the regulatory framework that controls copper homeostasis. To determine if this aspect of SCO1 function does in fact differ across tissues, we investigated its importance to copper homeostasis in the developing and adult heart using two relevant mouse models. We found that deletion of *Sco1* in both a heart and a striated muscle-specific knockout mouse was lethal, and that *Sco1* null hearts were both COX and copper deficient. However, unlike our previous findings in the *Sco1* null liver (38), the cardiac copper deficiency was caused by CTR1 mislocalisation rather than a reduction in its abundance. Disproportionate internalization of CTR1 in the absence of any changes in its steady-state levels was also observed in a $Sco1^{G115S/G115S}$ knockin mouse, an animal model of the human disease that results in an early onset, fatal cardiomyopathy in one of the three *SCO1* pedigrees (36). These data collectively support the concept that copper homeostasis is regulated by redox-dependent signaling through SCO1 in a tissue-specific manner.

Results

Generation of a heart-specific *Sco1* knockout mouse

The *SCO1* patient homozygous for the G132S mutation exhibited defects in cardiac physiology and presented with a lethal, neonatal cardiomyopathy (36). To better understand the mechanisms underlying the tissue-specific pathology and progression of this disease, we generated a transgenic mouse model in which *Sco1* was specifically deleted in the heart. Briefly, mice containing a pair of loxP sites flanking the second exon of the *Sco1* gene ($Sco1^{flox/flox}$) (38) were crossed to mice in which Cre recombinase expression is driven by the α−myosin heavy chain promoter (*Mhc-Cre*$^{tg/wt}$, Jackson #018972). Cre positive, F1 progeny (i.e. *Mhc-Cre*$^{tg/wt}$, $Sco1^{flox/wt}$) were then backcrossed to $Sco1^{flox/flox}$ animals to generate heart-specific *Sco1* knockout mice (*Mhc-Cre*$^{tg/wt}$, $Sco1^{flox/flox}$), hereafter referred to as $Sco1^{hrt/hrt}$ mice.

$Sco1^{hrt/hrt}$ mice were viable and all alleles were inherited at the expected Mendelian frequencies (data not shown). Although the birth weight of $Sco1^{hrt/hrt}$ mice was comparable to that of wild-type littermates (Supplementary Material, Fig. S1A), none survived beyond two days of age (Fig. 1A). PCR amplification of the *Sco1* locus in a number of somatic tissues confirmed that Cre-mediated excision events were restricted to the myocardium (Supplementary Material, Fig. S1B), and Western blot analysis demonstrated that the hearts of $Sco1^{hrt/hrt}$ mice had very low levels of SCO1 protein as early as embryonic day 15 (E15) (Fig. 1B).

$Sco1^{hrt/hrt}$ mice have a dilated cardiomyopathy owing to a severe, isolated COX deficiency

To further investigate the underlying basis of lethality in these animals, we first examined the $Sco1^{hrt/hrt}$ heart histologically. Hematoxylin and eosin staining revealed an enlarged left

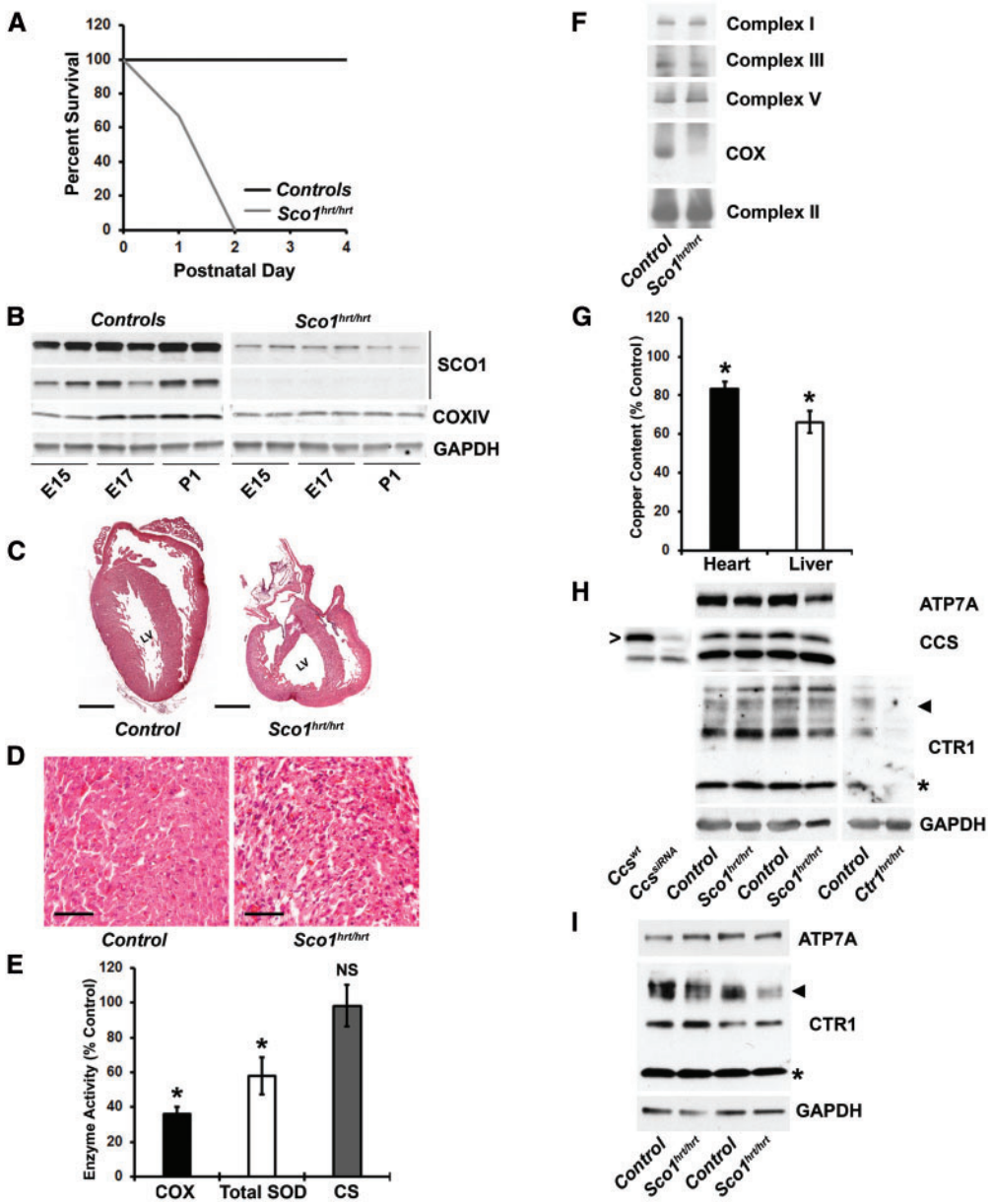

Figure 1. *Sco1*$^{hrt/hrt}$ mice present with a dilated cardiomyopathy owing to a severe, isolated COX deficiency. (**A**) Kaplan-Meier survival curve of wild-type (black) and *Sco1*$^{hrt/hrt}$ (grey) mice. (*Controls*, $n=40$; *Sco1*$^{hrt/hrt}$, $n=15$). (**B**) Western blot analysis of SCO1 and COX IV abundance in wild-type and *Sco1*$^{hrt/hrt}$ hearts at E15, E17 and P1. GAPDH was used as a loading control. (**C**) P1 wild-type (left) and *Sco1*$^{hrt/hrt}$ (right) hearts were stained with hematoxylin and eosin. LV denotes left ventricle, scale bar represents 500 μm. (**D**) 20X magnification of P1 wild-type (left) and *Sco1*$^{hrt/hrt}$ (right) hearts stained with hematoxylin and eosin. Scale bar represents 50 μm. (**E**) COX (P=0.04), total SOD (P=0.002) and CS activities in P1 *Sco1*$^{hrt/hrt}$ hearts expressed as a percentage of wild-type littermates (COX and CS, $n=3$ per genotype; total SOD, $n=6$ per genotype). (**F**) BN-PAGE analysis of the abundance of oxidative phosphorylation complexes in a P1 wild-type and *Sco1*$^{hrt/hrt}$ heart. (**G**) Total copper levels in the heart ($P=0.03$, $n=5$ per genotype) and liver ($P=0.01$, $n=3$ per genotype) of P1 *Sco1*$^{hrt/hrt}$ mice expressed as a percentage of wild-type littermates. (**H, I**) Western blot analysis of ATP7A, CTR1 and CCS abundance in hearts (H) and livers (I) of P1 wild-type and *Sco1*$^{hrt/hrt}$ mice. Hearts from *Ctr1*$^{flox/flox}$ and *Ctr1*$^{hrt/hrt}$ mice (53) were used as a reference control to identify the glycosylated (arrow) and truncated (asterisk) forms of CTR1. Mouse embryonic fibroblasts treated with scrambled (*Ccs*^{wt}) or *Ccs* siRNA (*Ccs*^{siRNA}) were also included as controls to identify the authentic species of CCS protein, which is denoted by the unfilled arrow. GAPDH was used as a loading control.

ventricle, indicative of a dilated cardiomyopathy (Fig. 1C). Negative Masson's trichrome staining (Fig. 1D) suggests that the ventricular dilation occurred in the absence of significant fibrosis. *Sco1*$^{hrt/hrt}$ hearts also exhibited a severe COX deficiency when compared with wild-type hearts (Fig. 1E, Supplementary Material, Fig. S1C). The COX deficiency was not accompanied by a change in the activity of citrate synthase (Fig. 1E) or the abundance of other OXPHOS complexes (Fig. 1F, Supplementary Material, Fig. S1C), suggesting that mitochondrial content remained unchanged in hearts that lack SCO1 expression.

A combined COX and copper deficiency is observed in affected *SCO1* patient tissues, and is a hallmark of the associated disease and its progression (36,38). Accordingly, the *Sco1*$^{hrt/hrt}$ heart had a slight, but statistically significant reduction in total copper content when compared with the wild-type heart (Fig. 1G), as well as a decrease in the total activity of superoxide

dismutase (SOD) (Fig. 1E) that was directly attributable to a reduction in the activity of the copper-dependent SOD1 form of the enzyme (Supplementary Material, Fig. S1D). Immunoblot analysis demonstrated that the mild copper deficiency in *Sco1*$^{hrt/hrt}$ hearts was not caused by changes in the total abundance of the copper import protein CTR1 or the copper export protein ATP7A (Fig. 1H). While total copper levels and CTR1 abundance were both significantly lower in the liver of *Sco1*$^{hrt/hrt}$ mice (Fig. 1G and I), there was no significant change in hepatic COX activity (Supplementary Material, Fig. S1E) or COX IV subunit abundance (Supplementary Material, Fig. S1F). The copper content of plasma and of other peripheral tissues of *Sco1*$^{hrt/hrt}$ mice was also comparable to wild-type littermates (Supplementary Material, Fig. S1G).

Striated-muscle specific *Sco1* knockout mice also develop a severe, dilated cardiomyopathy

The sudden perinatal lethality of the *Sco1*$^{hrt/hrt}$ mice precluded any meaningful investigation of disease progression owing to the loss of SCO1 function in the heart of this animal model. We therefore used a different Cre driver line in conjunction with the breeding strategy described above to generate striated muscle-specific *Sco1* knockout mice, hereafter referred to as *Sco1*$^{stm/stm}$ mice. *Sco1*$^{stm/stm}$ mice were born at the expected Mendelian frequency (data not shown), and Cre mediated excision at the *Sco1* locus was restricted to the striated muscle (Supplementary Material, Fig. S2A). *Sco1*$^{stm/stm}$ mice had a median lifespan of 100 days (Fig. 2A) without an observable change in their body weight (Supplementary Material, Fig. S2B). Unlike the hearts of *Sco1*$^{hrt/hrt}$ mice, SCO1 protein remained readily detectable in *Sco1*$^{stm/stm}$ hearts during the early postnatal period (Fig. 2B). Hearts from *Sco1*$^{stm/stm}$ mice were significantly larger at postnatal day 90 (P90), and weighed roughly 2-fold more than control hearts when normalized to body weight (Fig. 2C and D). P90 *Sco1*$^{stm/stm}$ cardiomyocytes were also markedly enlarged, vacuolated and displayed pronounced fibrosis (Fig. 2E), and expressed elevated transcript levels of markers of fetal reprogramming (Fig. 2F). To examine the impact of the observed histological and genetic changes on cardiac function, we next conducted non-invasive echocardiography imaging studies. Consistent with the observed dilated cardiomyopathy, P90 *Sco1*$^{stm/stm}$ hearts had a significantly increased left ventricular internal end-systolic diameter, and a corresponding reduction in ejection fraction and fractional shortening (Fig. 2G and H).

Dysfunction in *Sco1*$^{stm/stm}$ hearts is due to a combined COX and copper deficiency that worsens with age

To further investigate the underlying cause of the ventricular dilation in *Sco1*$^{stm/stm}$ mice, we characterized P90 hearts at a biochemical, molecular and elemental level. *Sco1*$^{stm/stm}$ hearts had a significant reduction in COX activity and COX IV protein levels when compared with the hearts of wild-type littermates (Fig. 3A and D, Supplementary Material, Fig. S2C). *Sco1*$^{stm/stm}$ hearts also exhibited a severe defect in total SOD activity (Fig. 3A) that was specific to the copper-dependent SOD1 form of the enzyme (Supplementary Material, Fig. S2D). Like *Sco1*$^{hrt/hrt}$ mice, the COX deficiency in *Sco1*$^{stm/stm}$ hearts was not caused by changes in mitochondrial content or remodelling, as the activity of citrate synthase (Fig. 3A) and the abundance of other OXPHOS complexes (Fig. 3B) remained unchanged. *Sco1*$^{stm/stm}$ hearts had significantly lower total copper levels than wild-type hearts, in the absence of changes in the total abundance of iron and zinc (Fig. 3C). None of the other somatic tissues of *Sco1*$^{stm/stm}$ mice we investigated exhibited altered copper, iron or zinc levels (Supplementary Material, Fig. S2E). Immunoblot analysis revealed that the severe copper deficiency in the P90 *Sco1*$^{stm/stm}$ heart was not attributable to a reduction in CTR1 abundance (Fig. 3D).

To more thoroughly characterize disease progression and the underlying cause of the copper deficiency in the *Sco1*$^{stm/stm}$ heart, we next investigated wild-type and *Sco1*$^{stm/stm}$ hearts at three earlier time points. At P18, *Sco1*$^{stm/stm}$ hearts exhibited a mild COX deficiency in the absence of a detectable change in total copper content (Fig. 4A and B). *Sco1*$^{stm/stm}$ hearts were both COX and copper deficient at P30, with the combined deficiency worsening significantly by P60 (Fig. 4A and B). Immunoblot analysis of wild-type and *Sco1*$^{stm/stm}$ hearts demonstrated that there was no difference in the total abundance of ATP7A (Fig. 4C), suggesting that the observed increase in ATP7A at P90 (Fig. 3D) occurs well after the initial onset of the copper deficiency. The abundance of CCS, a known biomarker of cytoplasmic copper status (39), was also unchanged. Interestingly, steady-state levels of CTR1 were elevated in response to *Sco1* deletion, even at P18 when total cardiac copper content is comparable across genotypes (Fig. 4B and C). These data collectively suggest that the copper deficiency in *Sco1*$^{stm/stm}$ hearts is caused by loss of CTR1 copper import activity rather than its degradation.

Copper deficiency in *Sco1*$^{stm/stm}$ and *Sco1*$^{G115S/G115S}$ knockin hearts is caused by mislocalisation of CTR1 to endosomes

We directly addressed the possibility that the cellular CTR1 pool was inappropriately distributed due to loss of SCO1 function by analysing wild-type and *Sco1*$^{stm/stm}$ hearts from P60 animals by indirect immunofluorescence. We found that in the wild-type heart CTR1 was primarily localized to the plasma membrane, with intense fluorescence at the intercalated discs, a pattern that was coincident with the plasma membrane marker protein Na^+/K^+ ATPase (Fig. 5). In contrast, CTR1 immunofluorescence was more diffuse in its distribution and less coincident with the Na^+/K^+ ATPase in the *Sco1*$^{stm/stm}$ heart (Fig. 5).

To compare and contrast the tissue-specific knockout with the human condition, we created a homozygous *Sco1*$^{G115S/G115S}$ knockin mouse to model the *SCO1* patient who presented neonatally with a fatal hypertrophic cardiomyopathy (36). *Sco1*$^{G115S/G115S}$ hearts exhibited a severe, combined COX and copper deficiency, like the knockout mouse model (Fig. 6A and B). The copper deficiency was not attributable to changes in the steady-state levels of CTR1 or ATP7A, and was not accompanied by changes in CCS abundance (Fig. 6B). Further mirroring the *Sco1*$^{stm/stm}$ heart, CTR1 was predominantly observed within the cytoplasm of the *Sco1*$^{G115S/G115S}$ heart, rather than at the plasma membrane and intercalated disks (Fig. 6C).

These data strongly suggest that perturbation of cardiac SCO1 function causes a copper deficiency by impairing CTR1 trafficking to, or maintenance at, the plasma membrane.To distinguish between these two possibilities, we co-stained wild-type and *Sco1*$^{stm/stm}$ hearts from P60 animals with antibodies raised against CTR1 and Rab5, an early endosomal marker. We found that internalized CTR1 convincingly co-localized with Rab5 in the *Sco1*$^{stm/stm}$ heart (Supplementary Material, Fig. S3A). However, follow-up imaging experiments failed to detect significant co-localization of CTR1 with either EEA1, a Rab5 effector

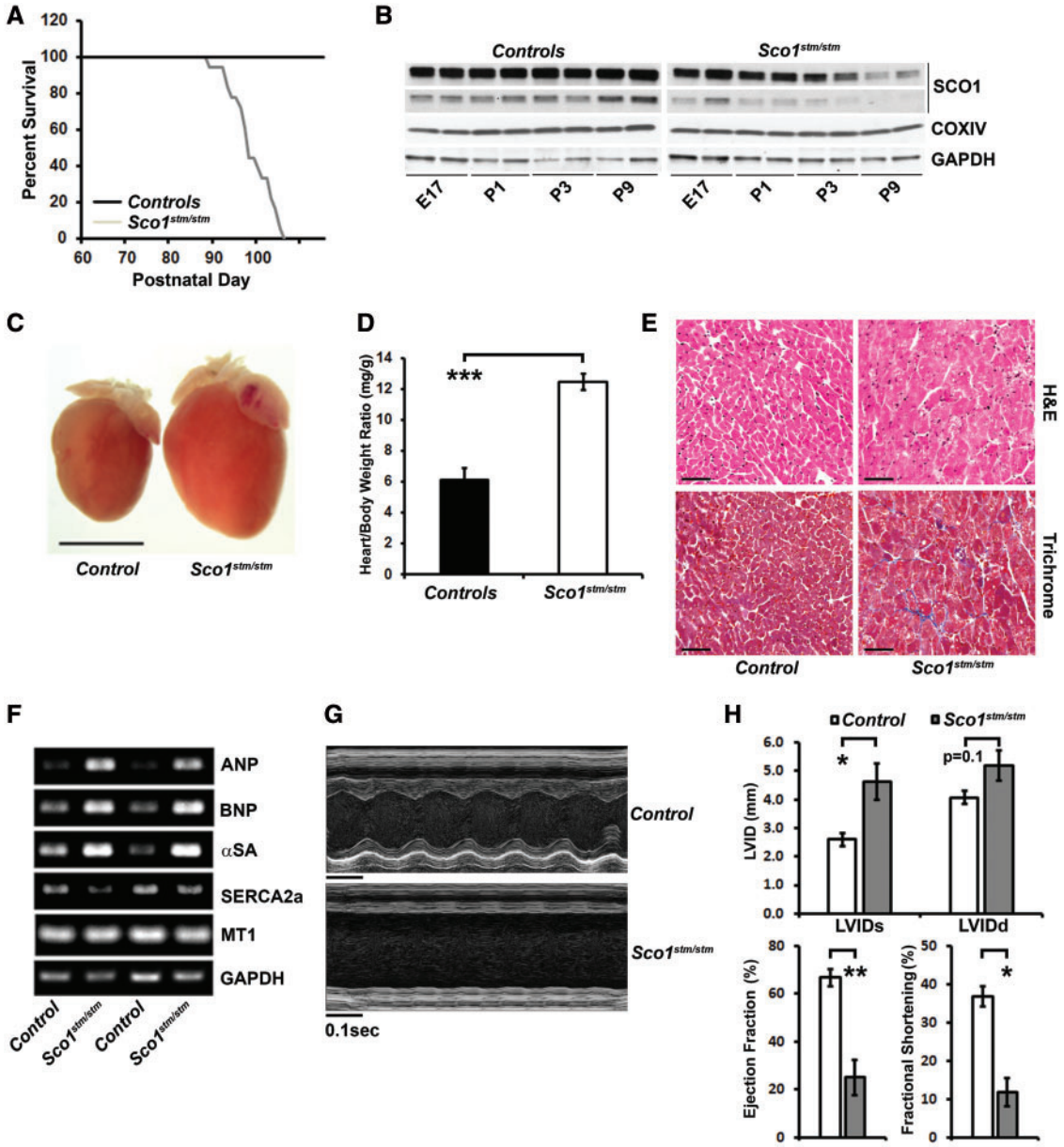

Figure 2. *Sco1*$^{stm/stm}$ mice also develop a severe, dilated cardiomyopathy. (**A**) Kaplan-Meier survival curve of wild-type (black) and *Sco1*$^{stm/stm}$ (grey) mice (*Controls*, $n = 22$; *Sco1*$^{stm/stm}$, $n = 18$). (**B**) Western Blot analysis of SCO1 and COX IV abundance in wild-type and *Sco1*$^{stm/stm}$ hearts at E17, P1, P3 and P9. GAPDH was used as a loading control. (**C**) 2X magnification of wild-type (left) and *Sco1*$^{stm/stm}$ (right) hearts at P90. Scale bar represents 1 cm. (**D**) Heart to body weight ratio for wild-type and *Sco1*$^{stm/stm}$ mice ($P = 0.0006$, $n = 7$ per genotype). (**E**) 20X magnification of P90 hearts from wild-type (left) and *Sco1*$^{stm/stm}$ (right) mice stained with hematoxylin and eosin (top) and Masson's trichrome stain (bottom). Scale bar represents 50 μm. (**F**) Semi-quantitative RT-PCR analysis of ANP, BNP, α−SA, SERCA2a and MT1 transcript levels. GAPDH was used as a loading control. (**G**) Representative echocardiogram comparing left ventricular function in P90 control (top) and *Sco1*$^{stm/stm}$ (bottom) mice. Scale bar represents 0.1 s. (**H**) Left ventricular internal diameter end systolic (LVIDs, $P = 0.05$), left ventricular internal diameter end diastolic (LVIDd, $P = 0.13$), fractional shortening ($P = 0.002$) and ejection fraction ($P = 0.006$) in P90 control and *Sco1*$^{stm/stm}$ hearts ($n = 4$ per genotype). No differences in these parameters were observed between wild-type and *Sco1*$^{stm/stm}$ hearts at P60 (data not shown).

and early endosomal marker, or LAMP1, a late endosomal/lysosomal marker (Supplementary Material, Fig. S3B). These data argue that loss of SCO1 function in the heart leads to CTR1 endocytosis from the plasma membrane.

Discussion

One of the puzzling hallmarks of disease in *SCO1* patients is the tissue-specific clinical presentation and, in particular, the differential susceptibility of the liver, brain or heart among *SCO1* pedigrees (30,36,37). SCO1 is an essential, ubiquitously expressed protein whose function couples the metallation of the Cu_A site of COX to the regulation of cellular copper homeostasis (28,34,36,40). How mitochondrial signaling in individual tissues is integrated into the regulatory framework that controls copper homeostasis remains unclear. To further explore this issue, and to build on our earlier work on a *Sco1* mouse model of the human disease caused by liver failure (38), we generated two mouse models that lacked *Sco1* expression in the heart. In both models, deletion of *Sco1* was ultimately lethal, thus

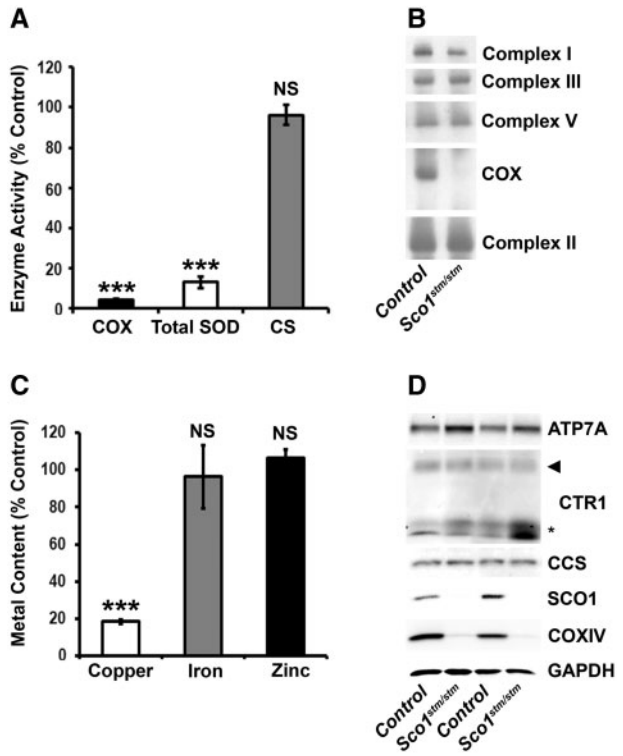

Figure 3. Dysfunction in *Sco1*$^{stm/stm}$ hearts is due to a combined COX and copper deficiency. (**A**) COX ($P = 0.00008$), total SOD ($P = 0.00008$) and CS activities in P90 *Sco1*$^{stm/stm}$ hearts expressed as a percentage of wild-type littermates ($n = 6$ per genotype for all enzymes). (**B**) BN-PAGE analysis of the abundance of oxidative phosphorylation complexes in P90 wild-type and *Sco1*$^{stm/stm}$ hearts. (**C**) Total copper ($P = 0.0002$), iron and zinc levels in P90 *Sco1*$^{stm/stm}$ hearts expressed as a percentage of wild-type littermates. ($n = 3$ per genotype for all metals). (**D**) Western Blot analysis of ATP7A, CTR1, SCO1, CCS and COXIV abundance in hearts of P90 wild-type and *Sco1*$^{stm/stm}$ mice. GAPDH was used as a loading control. The arrow and the asterisk denote the glycosylated and truncated forms of CTR1, respectively.

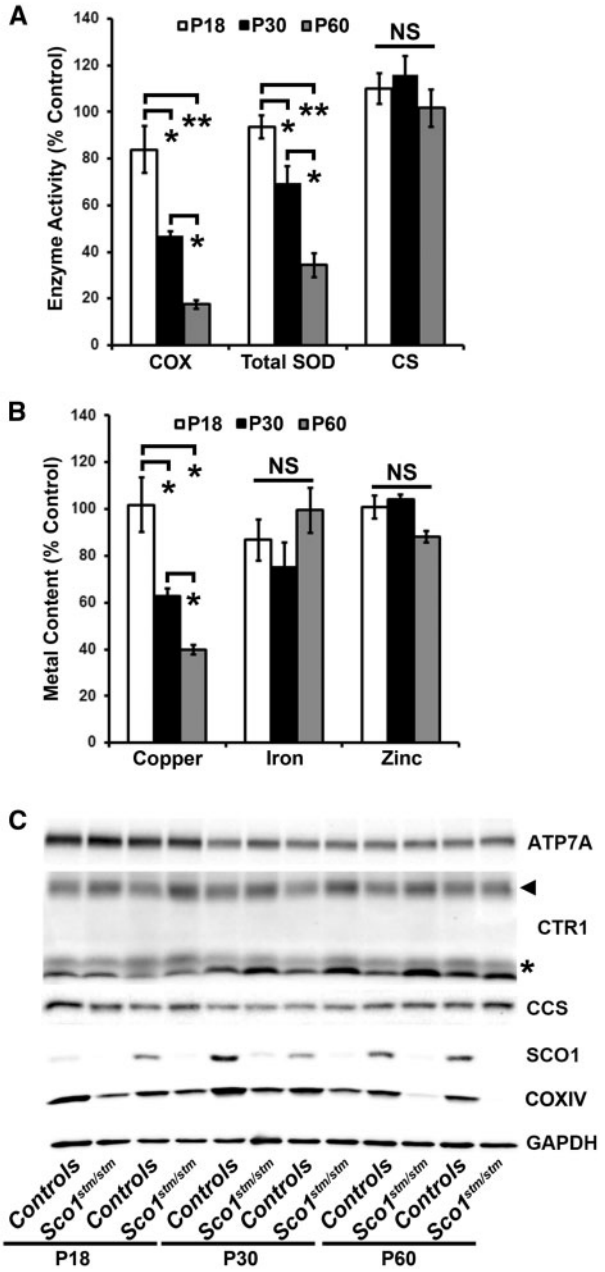

Figure 4. The combined COX and copper deficiency in *Sco1*$^{stm/stm}$ hearts worsens with age. (**A**) COX, total SOD and CS activities in *Sco1*$^{stm/stm}$ hearts at P18, P30 and P60 expressed as a percentage of age-matched hearts of wild-type littermates ($n = 3$ per genotype for all timepoints). (**B**) Total copper, iron and zinc levels in *Sco1*$^{stm/stm}$ hearts at P18, P30 and P60 expressed as a percentage of age-matched hearts of wild-type littermates ($n = 3$ per genotype for all timepoints). (**C**) Western blot analysis of ATP7A, CTR1, SCO1, CCS and COX IV abundance in hearts of P18, P30 and P60 *Sco1*$^{stm/stm}$ mice and wild-type littermates. GAPDH was used as a loading control. The arrow and the asterisk denote the glycosylated and truncated forms of CTR1, respectively.

demonstrating the importance of SCO1 function to the developing and adult myocardium.

A dilated cardiomyopathy owing to a combined COX and copper deficiency was manifest in both mouse models. SCO1 abundance was exceedingly low in the hearts of *Sco1*$^{hrt/hrt}$ mice as early as E15, and continued to drop postnatally. In contrast, SCO1 was readily detectable in the hearts of *Sco1*$^{stm/stm}$ mice up to P3. It is therefore likely that in this model there was sufficient residual SCO1 to support the development and rapid growth of the heart during this early perinatal window. Consistent with this idea, P18 *Sco1*$^{stm/stm}$ hearts only exhibited a mild COX deficiency relative to wild-type littermates. We cannot, however, discount the possibility that changes in the skeletal muscle also contributed to the longer lifespan in *Sco1*$^{stm/stm}$ mice, as a previous study elegantly demonstrated that simultaneous deletion of an unrelated mitochondrial gene in the heart and skeletal muscle contributed to a sparing effect on the heart itself (41). Hearts from both *Sco1*$^{hrt/hrt}$ and *Sco1*$^{stm/stm}$ mice were comprised of enlarged and vacuolated cardiomyocytes, and *Sco1*$^{stm/stm}$ hearts exhibited profound fibrosis and changes in the expression of multiple markers for fetal cardiac remodeling, presumably owing to their longer lifespan. These data combined with the significant increase in heart to body weight ratio and the dilation of the left ventricle observed by echocardiography suggest a dilated cardiomyopathy with mild cardiac hypertrophy in the P90 *Sco1*$^{stm/stm}$ heart.

Multiple lines of evidence strongly suggest that the primary factor for the copper deficiency in the *Sco1*$^{stm/stm}$ and *Sco1*$^{G115S/G115S}$ hearts is the mislocalisation of CTR1. In the wild-type heart, CTR1 is localized primarily to the plasma membrane with particularly intense staining at the intercalated discs.

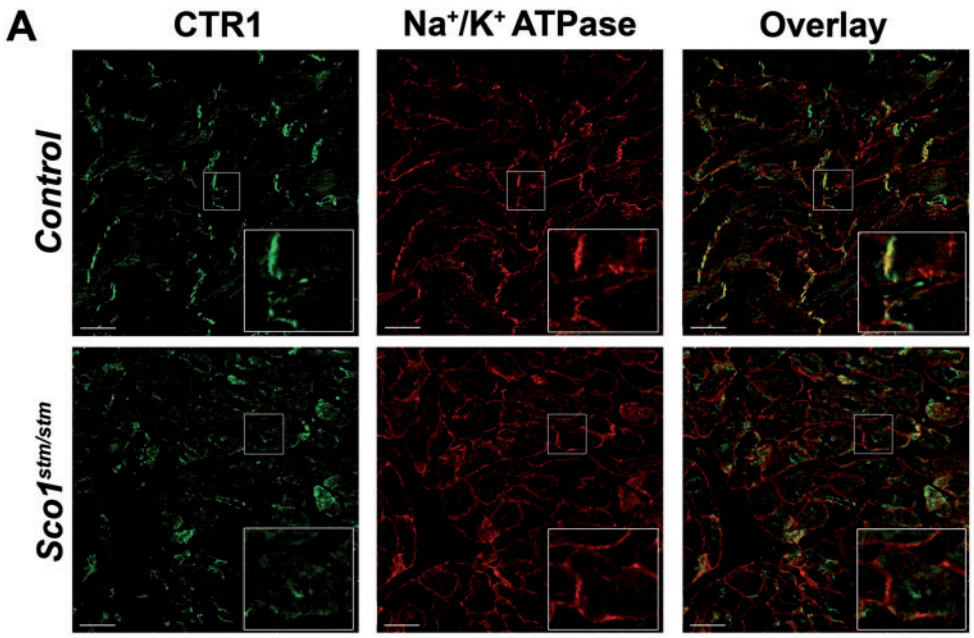

Figure 5. CTR1 is mislocalized in *Sco1*$^{stm/stm}$ hearts. Immunofluorescence analysis of CTR1 localisation in P60 wild-type (top) and *Sco1*$^{stm/stm}$ (bottom) hearts. Images were taken at 40X magnification and the plasma membrane marker Na^+/K^+ ATPase was used as a positive control. Scale bar represents 20 μm. Inset contains magnified image of selected region of interest (white box). Identical results were obtained with a second pair of P60 hearts (data not shown).

These data corroborate the findings of an earlier study in the heart (42), and suggest that CTR1 facilitates copper transport between cardiomyocytes at these cell-cell junctions, similar to other ions and metabolites (43–45). In contrast, CTR1 abundance at the intercalated disc was greatly attenuated in the *Sco1*$^{stm/stm}$ heart, where the protein was primarily localized to punctate intracellular structures found within the cytosol. CTR1-positive intracellular structures co-localized significantly with Rab5, but not with EEA1 or LAMP1. There is emerging evidence of an alternative endocytic pathway where relatively long-lived, Rab5-positive early endosomes contain the effectors APPL1 and APPL2 rather than EEA1 (46,47). Though these endosomes can be discriminated from the canonical EEA1-positive, early endosomes and are known to play important roles in storage, trafficking and signal transduction, their biological properties remain largely unknown (46,47). Our results raise the intriguing possibility that CTR1 is internalized in APPL-positive vesicles, although future studies will be required to confirm that loss of cardiac SCO1 function promotes CTR1 internalization via this alternate pathway. Similar intracellular redistribution of the total CTR1 pool away from the plasma membrane and intercalated disks was also observed in a heart homozygous for the SCO1 G115S substitution, the same allelic variant that in humans results in a hypertrophic cardiomyopathy (36). These data collectively argue that loss of SCO1 function in the heart causes a copper deficiency by impairing CTR1 localisation to the plasma membrane and therefore copper uptake into the cardiomyocyte.

Yet another intriguing finding of the present study is that perturbing the function of SCO1 in cardiomyocytes has a fundamentally different effect on CTR1 than it does in other cell types. Deletion of *Sco1* in both murine liver and embryonic fibroblasts promotes the degradation of CTR1, leading to a significant reduction in its steady-state levels (38). In contrast, *Sco1*$^{stm/stm}$ and *Sco1*$^{G115S/G115S}$ hearts have wild-type CTR1 abundance but fail to maintain adequate levels of the protein at the plasma membrane and intercalated disks to support copper import as evidenced by cardiac copper deficiency in these animals. The glycine to serine substitution in both mouse (unpublished data) and human SCO1 (36,37) does not completely abolish protein function, and allows for a longer lifespan in the *Sco1*$^{G115S/G115S}$ mice. Nonetheless, CTR1 is still mislocalized in the *Sco1*$^{G115S/G115S}$ heart, arguing that the effects we observe on CTR1 in the *Sco1*$^{stm/stm}$ heart are not simply a consequence of *Sco1* ablation and the resultant reduction in COX activity. While we do not yet know why perturbing SCO1-dependent mitochondrial signaling has distinct effects on CTR1 in the heart and liver, it may reflect different copper requirements in these tissues. Indeed, tissue-specific deletion of *Ctr1* in the heart is associated with rapid cardiac hypertrophy and lethality (48,49), suggesting a continuous need for CTR1-mediated copper uptake by cardiomyocytes and, by extension, little storage capacity. Therefore, it may be necessary in the heart to acutely regulate the localization rather than the steady-state levels of CTR1 in the face of *Sco1* deletion, to allow for more rapid responses to intrinsic changes in copper demand or extrinsic fluctuations in plasma copper levels. In contrast, the liver is a copper storage organ with higher total copper concentrations than the heart (34,50,51).Thus, degradation of CTR1 rather than recycling in response to *Sco1* deletion may reflect the relative abundance of copper in this organ or the existence of alternative pathways of copper acquisition. Consistent with this hypothesis, tissue-specific deletion of *Ctr1* in the liver during the postnatal period is associated with very mild hepatic copper deficiency and normal longevity (52).

How the loss of SCO1 function alters CTR1 localization in the heart while promoting CTR1 degradation in the liver remains an open question. Differences in redox balance between these two organs may contribute to the observed tissue-specific consequences of perturbing SCO1-dependent mitochondrial signaling on CTR1 function. The severe COX deficiency in *Sco1* null livers

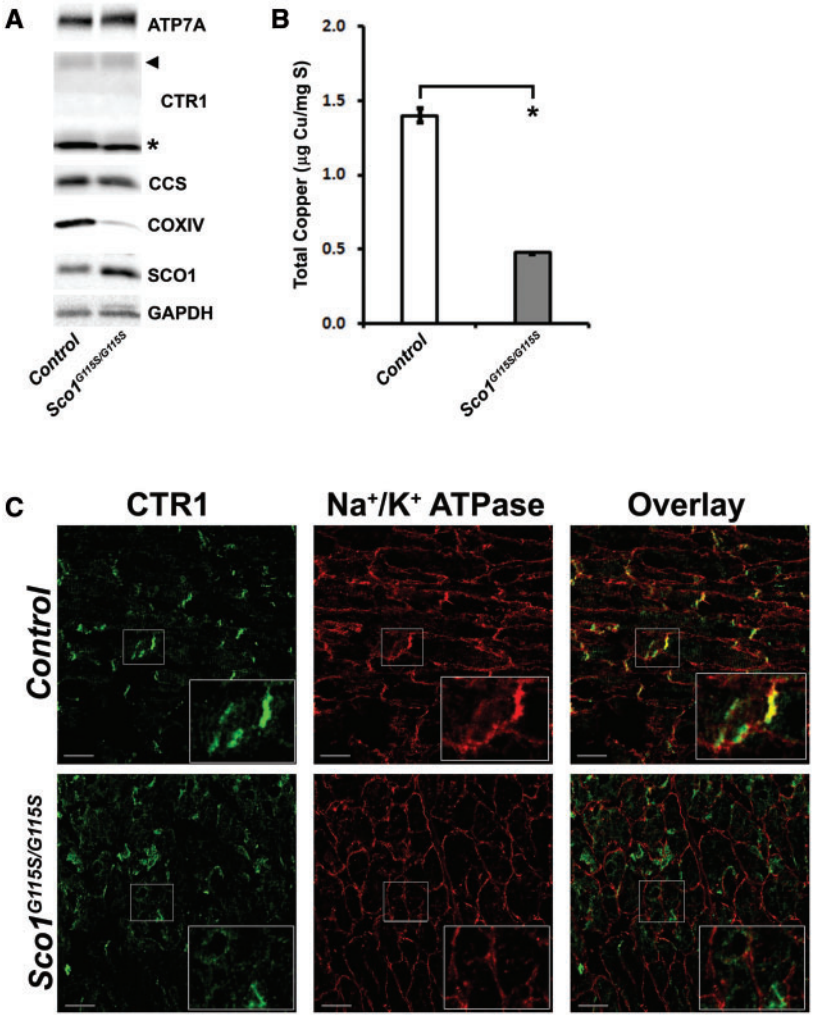

Figure 6. *Sco1*$^{G115S/G115S}$ knockin mice exhibit a severe copper deficiency that is also caused by the mislocalisation of CTR1. (**A**) Western blot analysis of ATP7A, CTR1, SCO1, CCS and COX IV abundance in P120 hearts of wild-type and *Sco1*$^{G115S/G115S}$ mice. GAPDH was used as a loading control. The arrow and the asterisk denote the glycosylated and truncated forms of CTR1, respectively. (**B**) Total copper levels (µg copper/mg sulphur [S]) in P120 *Sco1*$^{G115S/G115S}$ and wild-type hearts. (**C**) Immunofluorescence analysis of CTR1 localisation in P120 wild-type (top) and *Sco1*$^{G115S/G115S}$ (bottom) hearts. Images were taken at 40X magnification, and the plasma membrane marker Na^+/K^+ ATPase was used as a positive control. Scale bar represents 20 µm. Inset contains magnified image of selected region of interest (white box).

and hearts likely leads to oxidative stress. However, the metabolic poise and redox buffering capacity of each of these tissues is significantly different (53,54), and both of these factors may modulate the rate or nature of the signal that is transduced from the mitochondrion and sensed by other copper handling machinery. Signaling may also involve the release of one or more soluble, tissue-specific factors from the organelle that then acts to regulate CTR1 trafficking or degradation (28,40). Alternatively, loss of SCO1 function may affect signaling mediated by copper fluxes between mitochondria and the cytosol in a cell-type specific manner. Consistent with this idea, perturbing SCO1 function in the liver but not the heart alters the abundance of CCS (38), the only known biomarker of cytosolic copper status (39).

The reduction in hepatic copper levels in our *Sco1*$^{hrt/hrt}$ mouse model is an equally intriguing observation and points to crosstalk between the two tissues. Indeed, our findings mirror many aspects of those from an earlier study in which the high affinity copper importer *Ctr1* was deleted in the heart using the same Cre driver line (55). Because CTR1 is the only high affinity copper importer, we favour the idea that the COX-deficient *Ctr1*$^{hrt/hrt}$ heart is signaling to the liver in an attempt to correct this metabolic defect. Kim *et al.* (55) in fact demonstrate that CCS abundance is very high in the *Ctr1*$^{hrt/hrt}$ heart, suggesting that the organ is appropriately sensing a copper-deficient state in these animals. They then go on to show that there is a soluble factor in the plasma of *Ctr1*$^{hrt/hrt}$ mice that drives hepatic mobilization of copper into the circulation by increasing the steady-state levels of ATP7A. Mobilization of hepatic copper stores is consistent with one of the known roles of the liver in early perinatal life, which is to distribute copper and other essential metal ions to peripheral tissues to support organogenesis, and in the *Ctr1*$^{hrt/hrt}$ mouse is presumably occurring at a disproportionate rate in an attempt to rescue the failing and copper-deficient myocardium. In our *Sco1*$^{hrt/hrt}$ mouse model, however, liver ATP7A abundance and plasma copper levels are normal, and none of the peripheral tissues we examined have increased copper levels. CCS abundance is also unchanged in the *Sco1*$^{hrt/hrt}$ heart, leading us to speculate

that deletion of *Sco1* in the heart in this mouse model somehow signals a state of copper overload that is communicated to the liver and results in reduced CTR1 levels and increased excretion of copper in the bile.

Our findings emphasize the essential role of SCO1 in the mitochondrial regulation of copper homeostasis in both the developing and adult myocardium. They also strongly suggest that tissue-specific factors impinge upon how organelle signaling is sensed and integrated into the regulatory framework that controls copper homeostasis. Studies to identify the mechanistic basis that underpins the modulation of SCO1-dependent mitochondrial signaling in different tissues are on-going.

Materials and Methods

Generation of *Sco1* mouse models

Conditional *Sco1* knockout models were generated by crossing *Sco1* floxed mice ($Sco1^{flox/flox}$) (38) with mice in which Cre recombinase expression is driven by the α-myosin heavy chain (The Jackson Laboratory, strain #018972) or the creatine kinase promoter (The Jackson Laboratory, strain #006475). Cre positive, F1 progeny were then backcrossed to $Sco1^{flox/flox}$ animals to generate heart-specific ($Sco1^{hrt/hrt}$) or striated muscle-specific ($Sco1^{stm/stm}$) *Sco1* knockout mice. PCR genotyping of all animals in this breeding scheme was performed as previously described (38).

$Sco1^{G115S/wt}$ knockin mice were generated fee-for-service at the Toronto Centre for Phenogenomics. Briefly, the guide RNA 5'-GCATTAGCAAGCCTTTACTA-3', a single-strand oligonucleotide repair template with a silent mutation to disrupt the protospacer adjacent motif sequence, and *Cas9* mRNA were co-injected into C57BL/6NCrl zygotes. Resultant pups were screened by sequencing end-point PCR products to identify the point mutation, and bred to C57BL/6NCrl for germline transmission of the knockin allele. $Sco1^{G115S/wt}$ knockin mice were then backcrossed to C57BL/6NCrl animals for 3 successive generations to reduce the likelihood of animals carrying second site, off target mutations. $Sco1^{G115S/wt}$ knockin mice were intercrossed, and then bred with $Sco1^{G115S/G115S}$ knockin mice to both maintain a breeding colony and generate experimental animals. Tail DNA was prepared with the KAPA Mouse Genotyping Kit (KAPA Biosystems, KK5621), and 2 μl of a 1: 1 dilution in water was used in a 10 μl real-time PCR reaction with PerfeCTa qPCR ToughMix (VWR, CA97065-966) on the Applied Biosystems Step One Plus Real Time Thermocycler. The PCR reaction mix contained 500 nM of primers (F: TTAGAGCTGGAGAAACAACGG, R: GGCTCTCCATTGTGAGTTGTA) and 250 nM of probes (wild-type HEX probe, CA + TT + g+G + gAA + GCC and G115S knockin FAM probe, CA + TT + a+G + cAA + G+CCT) purchased from Integrated DNA Technologies, and was run for 40 cycles with an annealing temperature of 60 °C. All animal-related experiments were approved by the Animal Ethics Review Board at the University of Saskatchewan (AUP #20100091).

Echocardiography

The procedure for the mouse echocardiogram is described in detail elsewhere (56). In brief, cardiac function of wild-type and $Sco1^{stm/stm}$ mice ($n = 4$) was evaluated at P60 and P90 using a high resolution Vevo 2100 ultrasound system (VisualSonics, Toronto, ON, Canada) equipped with an MS550 transducer. Mice were anaesthetized using 3% isoflurane for 1–2 min, and then maintained at 1.5–2% isoflurane after losing the righting reflex. Mice were laid supine on a heated platform during echocardiography. Left ventricle internal diameter end systole (LVIDs) and diastole (LVIDd), fractional shortening and ejection fraction were measured from the standard LV short-axis M-mode view. The heart rate, electrocardiogram (ECG), respiratory rate and body temperature of the mouse were monitored throughout the experiment.

Tissue preparation and immunohistochemistry

Hearts from $Sco1^{hrt/hrt}$ mice and wild-type littermates were fixed *in situ* using 10% formalin for at least 48 h, dissected out of the chest cavity and embedded in paraffin. Hearts from $Sco1^{stm/stm}$ mice and wild-type littermates were dissected from the chest cavity and promptly perfused with HEPES buffered Tyrode's solution [25 mM HEPES (pH 7.4), 119 mM NaCl, 5 mM KCl, 2 mM $CaCl_2$, 2 mM $MgCl_2$ and 33 mM glucose] using a modified Langendorff setup. For hematoxylin and eosin and Masson's Trichrome staining, additional $Sco1^{stm/stm}$ hearts were fixed in 10% formalin for at least 48 h and embedded in paraffin. Hearts from both mouse models were sectioned into six micron slices, and slide mounted for staining. For immunofluorescent imaging, hearts from wild-type, $Sco1^{stm/stm}$ and $Sco1^{G115S/G115S}$ knockin mice were perfused as above, rapidly contact frozen in optical cutting temperature compound with dry ice chilled isobutane and stored at − 80 °C. Six micron frozen slices were sectioned with a cryostat and slide mounted. Slides were fixed post-sectioning for 10 min in acetone chilled to − 20 °C, washed twice for 5 min in phosphate buffered saline [PBS (pH 7.4); 2.7 mM KCl, 134 mM NaCl, 1.5 mM KH_2PO_4, 8 mM K_2HPO_4] and then once with 25 mM glycine for 10 min. For Rab5 and CTR1 stained slides, a permeabilization step (PBS + 0.1% Triton X-100) was added prior to blocking. Slides were blocked for 1 h in PBS containing 10% goat serum and 6% bovine serum albumin, and incubated overnight in a humidified chamber at 4 °C in antibody buffer [1X sodium/sodium citrate buffer (0.15 mM NaCL and 15 mM $Na_3C_6H_5O_72H_2O$), 2% goat serum, 1% BSA, 0.05% Triton X-100, 0.02% NaN_3] containing primary antibodies (1: 100) raised against the Na^+/K^+ ATPase (Millipore), CTR1 (kind gift from Dr. Jack Kaplan, University of Illinois at Chicago, USA), Rab5 (Abcam), EEA1 (BD Biosciences) and/or LAMP1 (Santa Cruz Biotechnology). Slides were then washed twice more in PBS for 5 min and incubated at room temperature in a humidified chamber for 1 h in secondary antibodies [Abcam: anti-Rat IgG Alexa Fluor 647 (1: 1000); Cell Signaling Technologies: anti-Rabbit IgG Alexa Fluor 488 (1: 1000) and anti-Mouse IgG Alexa Fluor 594 (1: 750)] in antibody dilution buffer. Finally, the slides were washed twice with PBS for 5 min. All imaging was done using a ZEISS LSM-700 confocal microscope with image acquisition performed using ZEISS Zen Black imaging software.

Native and denaturing electrophoresis

Tissues from cervically dislocated mice were harvested and frozen at −80 °C. Blue native polyacrylamide gel electrophoresis (BN-PAGE) analyses were conducted as described in detail elsewhere (57). Briefly, a piece of heart tissue was resuspended and gently homogenized in extraction buffer [20 mM bis-Tris (pH 7.4), 50 mM NaCl, 10% (v/v) glycerol and 0.2% (w/v) lauryl maltoside]. The protein concentration was then quantified and adjusted to 2 mg/ml, and samples were incubated on ice for 30 min. Following a 5-min spin at 18 000 × *g* at 4 °C and the addition of loading dye, equal amounts of protein (20 μg/lane) were fractionated on a 6–16% acrylamide gradient gel and transferred

to a nitrocellulose membrane under semi-dry conditions. For denaturing electrophoresis, proteins were extracted from excised tissues by dounce homogenization in a RIPA extraction buffer [50 mM Tris (pH 7.4), 150 mM NaCl, 1% Triton X-100, 0.5% sodium deoxycholate, 0.1% SDS, 1 mM EDTA and 1x Complete protease inhibitor cocktail (Roche)], adjusted to a final concentration of 5 mg/ml, incubated on ice for 30 min and then centrifuged at 4 °C for 10 min at 12 000×*g*. Equal amounts of protein were separated on precast 4–20% SDS-PAGE gradient gels (BioRad), transferred to nitrocellulose membrane, blocked for 2 h in Tris buffered saline supplemented with Tween 20 [TBST; 25 mM Tris (pH 7.4), 137 mM NaCl, 2.5 mM KCl and 0.05% Tween 20] containing 5% milk (US Biologicals), and incubated overnight at 4 °C in primary monoclonal [Abcam, COX I (1: 1000), COX IV (1: 1000), Core 1 (1: 1000), ATPase α subunit (1: 1000), NDUFA9 (1: 1000), SDHA (1: 10000); Cell Signaling Technologies, GAPDH (1: 1, 000)] and polyclonal [CTR1 (1: 250, GenScript fee-for-service antibody production with peptide VSIRYNSMPVP GPNGTILC); CCS (1: 1: 000, kind gift from Dr. Joe Prohaska, University of Minnesota); SCO1 (1: 1, 000, in house fee-for-service antibody production with peptide CEKMIEVVE EIDSIPSLPNLT)] antibodies. Membranes were then washed six times for 5 min in TBST, incubated for 60 min in the appropriate horseradish peroxidase conjugated secondary antibody (Biorad, 1: 2500) in TBST containing 5% milk, and washed again in TBST as above. Membranes were developed using a homemade luminol-enhanced chemiluminescence solution, and visualized with X-ray film or the BioRad ChemiDoc^{TM} MP Imaging System.

RT-PCR analysis

Total RNA was isolated from hearts and reverse transcribed into cDNA, as previously described (38). PCR reactions contained equal amounts of cDNA and unique primer sets to generate the following amplicons; ANP (F: GCTTCCAGGCCATATTGGAG, R: GGGGGCATGACCTCATCTT), BNP (F: GAGGTCACTCCTATCCTC TGG, R: GCCATTTCCTCCGACTTTTCTC), α-SA (F: CCCAAAGC TAACCGGGAGAAG, R: CCAGAATCCAACACGATGCC), SERCA2 (F: TGGAACAACCCGGTAAAGAGT, R: CACCAGGGGCATAATGAGC AG), MT1 (F: GTCCTCTAAGCGTCACCAC, R: GAGCAGTTGGGG TCCATTC) and GAPDH (F: ATGGTGAAGGTCGGTGTGAA, R: GC CGTGAGTGGAGTCATACT)). PCR conditions were optimized to ensure the amplification of a single product was captured in the log phase of the reaction.

Miscellaneous

Elemental analyses, total protein quantitation and enzyme activity assays were performed as described in detail elsewhere (33). Where applicable, data were presented as the mean ± standard error of the mean, and significant differences between experimental groups were detected using a two-sample *t*-test assuming unequal variance. * denotes $P < 0.05$, ** denotes $P < 0.01$, *** denotes $P < 0.001$ and NS denotes not significant.

Supplementary Material

Supplementary Material is available at *HMG* online.

Acknowledgements

We are grateful to Drs. Timothy Wai (INEM, Paris, France) and Roman Polishchuk (TIGEM, Italy) for helpful discussions throughout the course of these studies, and Carmen Whitehead for mouse husbandry. We also would like to acknowledge Drs. Jack Kaplan (University of Illinois Chicago, USA) and Joe Prohaska (University of Minnesota, USA) for the CTR1 and CCS antisera, respectively.

Conflict of Interest statement. None declared.

Funding

Canadian Institutes of Health Research (CIHR) to SCL and a Canada Foundation for Innovation grant to GFT. KAJ is a Saskatchewan Health Research Foundation Postdoctoral fellow, SCL is a CIHR New Investigator awardee and GFT is a Canada Research Chair. Funding to pay the Open Access publication charges for this article was provided by the Canadian Institutes of Health Research.

References

1. Nevitt, T., Ohrvik, H. and Thiele, D.J. (2012) Charting the travels of copper in eukaryotes from yeast to mammals. *Biochim. Biophys. Acta*, **1823**, 1580–1593.
2. Kim, B.E., Nevitt, T. and Thiele, D.J. (2008) Mechanisms for copper acquisition, distribution and regulation. *Nat. Chem. Biol.*, **4**, 176–185.
3. Macomber, L. and Imlay, J.A. (2009) The iron-sulfur clusters of dehydratases are primary intracellular targets of copper toxicity. *Proc. Natl. Acad. Sci.*, **106**, 8344–8349.
4. Brancaccio, D., Gallo, A., Piccioli, M., Novellino, E., Ciofi-Baffoni, S. and Banci, L. (2017) [4Fe-4S] cluster assembly in mitochondria and its impairment by copper. *J. Am. Chem. Soc.*, **139**, 719–730.
5. Jomova, K. and Valko, M. (2011) Advances in metal-induced oxidative stress and human disease. *Toxicology*, **283**, 65–87.
6. Stohs, S.J. and Bagchi, D. (1995) Oxidative mechanisms in the toxicity of metal ions. *Free Radic. Biol. Med.*, **18**, 321–336.
7. Rae, T.D., Schmidt, P.J., Pufahl, R.A., Culotta, V.C. and O'Halloran, T.V. (1999) Undetectable intracellular free copper: The requirement of a copper chaperone for superoxide-dismutase. *Science*, **284**, 805–808.
8. Tisato, F., Marzano, C., Porchia, M., Pellei, M. and Santini, C. (2010) Copper in diseases and treatments, and copper-based anticancer strategies. *Med. Res. Rev.*, **30**, 708–749.
9. Zhou, B. and Gitschier, J. (1997) hCTR1: A human gene for copper uptake identified by complementation in yeast. *Proc. Natl. Acad. Sci. USA*, **94**, 7481–7486.
10. Lee, J., Prohaska, J.R. and Thiele, D.J. (2001) Essential role for mammalian copper transporter Ctr1 in copper homeostasis and embryonic development. *Proc. Natl. Acad. Sci. USA*, **98**, 6842–6847.
11. Aller, S.G. and Unger, V.M. (2006) Projection structure of the human copper transporter CTR1 at 6-A resolution reveals a compact trimer with a novel channel-like architecture. *Proc. Natl. Acad. Sci. USA*, **103**, 3627–3632.
12. Amaravadi, R., Glerum, D.M. and Tzagoloff, A. (1997) Isolation of a cDNA encoding the human homolog of COX17, a yeast gene essential for mitochondrial copper recruitment. *Hum. Genet.*, **99**, 329–333.
13. Klomp, L.W., Lin, S.J., Yuan, D.S., Klausner, R.D., Culotta, V.C. and Gitlin, J.D. (1997) Identification and functional expression of HAH1, a novel human gene involved in copper homeostasis. *J. Biol. Chem.*, **272**, 9221–9226.
14. Culotta, V.C., Klomp, L.W., Strain, J., Casareno, R.L., Krems, B. and Gitlin, J.D. (1997) The copper chaperone for superoxide dismutase. *J. Biol. Chem.*, **272**, 23469–23472.

15. Flores, A.G. and Unger, V.M. (2013) Atox1 contains positive residues that mediate membrane association and aid subsequent copper loading. *J. Membr. Biol.*, **246**, 903–913.
16. Pope, C.R., De Feo, C.J. and Unger, V.M. (2013) Cellular distribution of copper to superoxide dismutase involves scaffolding by membranes. *Proc. Natl. Acad. Sci. USA*, **110**, 20491–20496.
17. Guo, Y., Smith, K., Lee, J., Thiele, D.J. and Petris, M.J. (2004) Identification of methionine-rich clusters that regulate copper-stimulated endocytosis of the human Ctr1 copper transporter. *J. Biol. Chem.*, **279**, 17428–17433.
18. Maryon, E.B., Molloy, S.A., Ivy, K., Yu, H. and Kaplan, J.H. (2013) Rate and regulation of copper transport by human copper transporter 1 (hCTR1). *J. Biol. Chem.*, **288**, 18035–18046.
19. Clifford, R.J., Maryon, E.B. and Kaplan, J.H. (2016) Dynamic internalization and recycling of a metal ion transporter: Cu homeostasis and CTR1, the human cu^{+} uptake system. *J. Cell. Sci.*, **129**, 1711–1721.
20. Klomp, A.E., Tops, B.B., Van Denberg, I.E., Berger, R. and Klomp, L.W. (2002) Biochemical characterization and subcellular localization of human copper transporter 1 (hCTR1). *Biochem. J.*, **364**, 497–505.
21. Tchaparian, E.H., Uriu-Adams, J.Y., Keen, C.L., Mitchell, A.E. and Rucker, R.B. (2000) Lysyl oxidase and P-ATPase-7A expression during embryonic development in the rat. *Arch. Biochem. Biophys.*, **379**, 71–77.
22. Petris, M.J., Strausak, D. and Mercer, J.F. (2000) The menkes copper transporter is required for the activation of tyrosinase. *Hum. Mol. Genet.*, **9**, 2845–2851.
23. El Meskini, R., Culotta, V.C., Mains, R.E. and Eipper, B.A. (2003) Supplying copper to the cuproenzyme peptidylglycine alpha-amidating monooxygenase. *J. Biol. Chem.*, **278**, 12278–12284.
24. Petris, M.J., Mercer, J.F., Culvenor, J.G., Lockhart, P., Gleeson, P.A. and Camakaris, J. (1996) Ligand-regulated transport of the menkes copper P-type ATPase efflux pump from the golgi apparatus to the plasma membrane: A novel mechanism of regulated trafficking. *embo J.*, **15**, 6084–6095.
25. Polishchuk, E.V., Concilli, M., Iacobacci, S., Chesi, G., Pastore, N., Piccolo, P., Paladino, S., Baldantoni, D., van IJzendoorn, S.C., Chan, J. *et al.* (2014) Wilson disease protein ATP7B utilizes lysosomal exocytosis to maintain copper homeostasis. *Dev. Cell*, **29**, 686–700.
26. Mercer, J.F., Livingston, J., Hall, B., Paynter, J.A., Begy, C., Chandrasekharappa, S., Lockhart, P., Grimes, A., Bhave, M. and Siemieniak, D. (1993) Isolation of a partial candidate gene for menkes disease by positional cloning. *Nat. Genet.*, **3**, 20–25.
27. Petrukhin, K., Lutsenko, S., Chernov, I., Ross, B.M., Kaplan, J.H. and Gilliam, T.C. (1994) Characterization of the wilson disease gene encoding a P-type copper transporting ATPase: Genomic organization, alternative splicing, and structure/function predictions. *Hum. Mol. Genet.*, **3**, 1647–1656.
28. Leary, S.C., Winge, D.R. and Cobine, P.A. (2009) "Pulling the plug" on cellular copper: The role of mitochondria in copper export. *Biochim. Biophys. Acta*, **1793**, 146–153.
29. Baertling, F., van den Brand, M., Hertecant, J.L., Al-Shamsi, A., van den Heuvel, L., Distelmaier, F., Mayatepek, E., Smeitink, J.A., Nijtmans, L.G. and Rodenburg, R.J. (2015) Mutations in COA6 cause cytochrome c oxidase deficiency and neonatal hypertrophic cardiomyopathy. *Hum. Mutat.*, **36**, 34–38.
30. Valnot, I., Osmond, S., Gigarel, N., Mehaye, B., Amiel, J., Cormier-Daire, V., Munnich, A., Bonnefont, J., Rustin, P. and Rötig, A. (2000) Mutations of the SCO1 gene in mitochondrial cytochrome c oxidase deficiency with neonatal-onset hepatic failure and encephalopathy. *Am. J. Hum. Genet.*, **67**, 1104–1109.
31. Papadopoulou, L.C., Sue, C., Davidson, M.M., Tanji, K., Nishino, I., Sadlock, J.E., Krishna, S., Walker, W., Selby, J., Glerum, D.M. *et al.* (1999) Fatal infantile cardioencephalomyopathy with COX deficiency and mutations in SCO2, a COX assembly gene. *Nat. Genet.*, **23**, 333–337.
32. Horng, Y.C., Leary, S.C., Cobine, P.A., Young, F.B., George, G.N., Shoubridge, E.A. and Winge, D.R. (2005) Human Sco1 and Sco2 function as copper-binding proteins. *J. Biol. Chem.*, **280**, 34113–34122.
33. Leary, S.C., Kaufman, B.A., Pellecchia, G., Guercin, G.H., Mattman, A., Jaksch, M. and Shoubridge, E.A. (2004) Human SCO1 and SCO2 have independent, cooperative functions in copper delivery to cytochrome c oxidase. *Hum. Mol. Genet.*, **13**, 1839–1848.
34. Leary, S.C., Cobine, P.A., Kaufman, B.A., Guercin, G.H., Mattman, A., Palaty, J., Lockitch, G., Winge, D.R., Rustin, P., Horvath, R. *et al.* (2007) The human cytochrome c oxidase assembly factors SCO1 and SCO2 have regulatory roles in the maintenance of cellular copper homeostasis. *Cell Metab.*, **5**, 9–20.
35. Leary, S.C., Cobine, P.A., Nishimura, T., Verdijk, R.M., de Krijger, R., de Coo, R., Tarnopolsky, M.A., Winge, D.R. and Shoubridge, E.A. (2013) COX19 mediates the transduction of a mitochondrial redox signal from SCO1 that regulates ATP7A-mediated cellular copper efflux. *Mol. Biol. Cell*, **24**, 683–691.
36. Stiburek, L., Vesela, K., Hansikova, H., Hulkova, H. and Zeman, J. (2009) Loss of function of Sco1 and its interaction with cytochrome c oxidase. *Am. J. Physiol. Cell Physiol.*, **296**, 1218–1226.
37. Leary, S.C., Antonicka, H., Sasarman, F., Weraarpachai, W., Cobine, P.A., Pan, M., Brown, G.K., Brown, R., Majewski, J., Ha, K.C. *et al.* (2013) Novel mutations in SCO1 as a cause of fatal infantile encephalopathy and lactic acidosis. *Hum. Mutat.*, **34**, 1366–1370.
38. Hlynialuk, C.J., Ling, B., Baker, Z.N., Cobine, P.A., Yu, L.D., Boulet, A., Wai, T., Hossain, A., El Zawily, A.M., McFie, P.J. *et al.* (2015) The mitochondrial Metallochaperone SCO1 Is required to sustain expression of the high-affinity copper transporter CTR1 and preserve copper homeostasis. *Cell Rep.*, **10**, 933–943.
39. Lassi, K.C. and Prohaska, J.R. (2012) Erythrocyte copper chaperone for superoxide dismutase is increased following marginal copper deficiency in adult and postweanling mice. *J. Nutr.*, **142**, 292–297.
40. Leary, S.C. (2010) Redox regulation of SCO protein function: Controlling copper at a mitochondrial crossroad. *Antioxid. Redox Signal*, **13**, 1403–1416.
41. Wai, T., García-Prieto, J., Baker, M.J., Merkwirth, C., Benit, P., Rustin, P., Rupérez, F.J., Barbas, C., Ibañez, B. and Langer, T. (2015) Imbalanced OPA1 processing and mitochondrial fragmentation cause heart failure in mice. *Science*, **350**, aad0116-1-aad0116-11.
42. Kuo, Y.M., Gybina, A.A., Pyatskowit, J.W., Gitschier, J. and Prohaska, J.R. (2006) Copper transport protein (Ctr1) levels in mice are tissue specific and dependent on copper status. *J. Nutr.*, **136**, 21–26.
43. Doria-Medina, C.L., Lund, D.D., Pasley, A., Sandra, A. and Sivitz, W.I. (1993) Immunolocalization of GLUT-1 glucose transporter in rat skeletal muscle and in normal and hypoxic cardiac tissue. *Am. J. Physiol.*, **265**, E454–E464.

44. Valiunas, V., Polosina, Y.Y., Miller, H., Potapova, I.A., Valiuniene, L., Doronin, S., Mathias, R.T., Robinson, R.B., Rosen, M.R., Cohen, I.S. *et al.* (2005) Connexin-specific cell-to-cell transfer of short interfering RNA by gap junctions. *J. Physiol.*, **568**, 459–468.
45. Kleber, A.G. and Saffitz, J.E. (2014) Role of the intercalated disc in cardiac propagation and arrhythmogenes. *Front. Physiol.*, **5**, 404.
46. Urbanska, A., Sadowski, L., Kalaidzidis, Y. and Miaczynska, M. (2011) Biochemical characterization of APPL endosomes: the role of Annexin A2 in APPL membrane recruitment. *Traffic*, **12**, 1227–1241.
47. Kalaidzidis, I., Miaczynska, M., Brewińska-Olchowik, M., Hupalowska, A., Ferguson, C., Parton, R.G., Kalaidzidis, Y. and Zerial, M. (2015) APPL endosomes are not obligatory endocytic intermediates but act as stable cargo-sorting compartments. *J. Cell Biol.*, **211**, 123–144.
48. Prohaska, J.R. (1983) Changes in tissue growth, concentrations of copper, iron, cytochrome oxidase and superoxide dismutase subsequent to dietary or genetic copper deficiency in mice. *J. Nutr.*, **113**, 2048–2058.
49. Nose, Y., Kim, B.E. and Thiele, D.J. (2006) Ctr1 drives intestinal copper absorption and is essential for growth, iron metabolism, and neonatal cardiac function. *Cell Metab.*, **4**, 235–244.
50. Camakaris, J., Mann, J.R. and Danks, D.M. (1979) Copper metabolism in mottled mouse mutants: Copper concentrations in tissues during development. *Biochem. J.*, **180**, 597–604.
51. Casey, C.E., Guthrie, B.E. and McKenzie, J.M. (1982) Trace elements in tissues from new zealanders: A compilation of published data. *N. Z. Med. J.*, **95**, 768–771.
52. Kim, H., Son, H.Y., Bailey, S.M. and Lee, J. (2009) Deletion of hepatic Ctr1 reveals its function in copper acquisition and compensatory mechanisms for copper homeostasis. *Am. J. Physiol. Gastrointest. Liver Physiol.*, **296**, 356–364.
53. Rebrin, I., Kamzalov, S. and Sohal, R.S. (2003) Effects of age and caloric restriction on glutathione redox state in mice. *Free Radic. Biol. Med.*, **35**, 626–635.
54. Rebrin, I. and Sohal, R.S. (2004) Comparison of thiol redox state of mitochondria and homogenates of various tissues between two strains of ice with different longevities. *Exp. Gerontol.*, **39**, 1513–1519.
55. Kim, B.E., Turski, M.L., Nose, Y., Casad, M., Rockman, H.A. and Thiele, D.J. (2010) Cardiac copper deficiency activates a systemic signaling mechanism that communicates with the copper acquisition and storage organs. *Cell Metab.*, **11**, 353–363.
56. Lee, L., Cui, J.Z., Cua, M., Esfandiarei, M., Sheng, X., Chui, W., Xu, M.H., Sarunic, M.V., Beg, M.F., van Breemen, C. *et al.* (2016) Aortic and cardiac structure and function using high-resolution echocardiography and optical coherence tomography in a mouse model of marfan syndrome. *PLoS One*, **11**, e0164778.
57. McKenzie, M., Lazarou, M., Thorburn, D.R. and Ryan, M.T. (2007) Analysis of mitochondrial subunit assembly into respiratory chain complexes using blue native polyacrylamide gel electrophoresis. *Anal. Biochem.*, **364**, 128–137.